Materials Science in Semiconductor Processing 63 (2017) 64–71

Contents lists available at ScienceDirect

Materials Science in Semiconductor Processing

journal homepage: www.elsevier.com/locate/mssp

The surface morphology, structural properties and chemical composition of $Cd_{1-x}Zn_xTe$ polycrystalline thick films deposited by close spaced vacuum sublimation

Y.V. Znamenshchykov[a,*], V.V. Kosyak[a], A.S. Opanasyuk[a], E. Dauksta[c], A.A. Ponomarov[b], A.V. Romanenko[b], A.S. Stanislavov[b], A. Medvids[c], I.O. Shpetnyi[a,d], Yu.I. Gorobets[d]

[a] Sumy State University, 2, Rymsky Korsakov Str., 40007 Sumy, Ukraine
[b] Institute of Applied Physics of the National Academy of Sciences of Ukraine, 58, Petropavlivska str., 40030 Sumy, Ukraine
[c] Riga Technical University, 3 Paula Valdena Str., LV-1048 Riga, Latvia
[d] Institute of Magnetism of the National Academy of Sciences of Ukraine and the Ministry of Education and Science of Ukraine, 36-b Vernadsky Ave., 03142 Kyiv, Ukraine

ARTICLE INFO

Keywords:
Semiconducting ternary compounds
X-ray diffraction
Crystal structure
Polycrystalline deposition
Solid solutions

ABSTRACT

Thick polycrystalline $Cd_{1-x}Zn_xTe$ films with x ranged from 0.37 to 0.80 were obtained by the close spaced vacuum sublimation method. In order to investigate properties of the films structural, PIXE and Raman studies were carried out. Determination of chemical composition of the films by EDS, PIXE and XRD has shown good correlation of results. Raman spectroscopy reveals the relation between zinc concentration and vibrational properties of the films. Studies of the spatial distribution of the chemical elements on the film surface by micro-PIXE and micro-Raman spectroscopy have shown that films are uniform and free of secondary phases such as CdTe, ZnTe and Te inclusions.

1. Introduction

The $Cd_{1-x}Zn_xTe$ (CZT) single crystals are widely used for room temperature detectors of the hard radiation [1–3]. It is possible due to such characteristics of CZT as high resistivity, high atomic number, high binding energy and tunable band gap in the range 1.50–2.26 eV depending on Zn concentration. However, it is difficult to obtain high-quality single crystals with $x > 0.10$ and uniform distribution of the chemical elements. Thus, the CZT crystals contain defects such as Te-precipitates, twins and dislocations [4,5], which lead to deterioration of detector properties.

Despite the fact that polycrystalline materials contain more structural defects than single crystals, the polycrystalline thick CZT films are also used as a detector material [6–9]. It is due to ability to produce low-cost, large-area flat panel detectors [8,10] based on thick films free of Te-inclusions with zinc concentration $x > 0.10$ and uniform zinc distribution [11]. At the same time application in electronic devices, especially fabrication of radiation detectors, requires high-quality CZT films with big grain size, high texture, low concentration of defects, and uniform distribution of chemical elements.

Distribution of secondary phases in CZT single crystals was studied by IR transmission microscopy [12,13], micro-photoluminescence [14] and micro-Raman spectroscopy [15,16].

The Raman spectroscopy is very sensitive to phase composition of materials. In particular, this method allows detecting Te-inclusions in CZT films and single crystals [12,15,16]. Also, the Raman spectroscopy was used for study of the distribution of chemical elements in epitaxial CdTe thin films [17]. However, the spatial distribution of secondary phases and chemical elements in thick polycrystalline CZT films has not been studied yet.

As a rule Raman spectra of cubic phase CZT include CdTe and ZnTe-related modes of longitudinal (LO) and transverse (TO) optical phonons. However, the presence of Te inclusions leads to the appearance of Te-related modes on Raman spectra of CZT films [18].

Particle-induced X-ray emission (PIXE) technique allows simultaneous determining the elemental concentrations of the major and trace elements of the samples without standards usage by detecting and processing the characteristic X-rays of elements induced by accelerated ion beam [19]. Usually in μ-PIXE the H+ beam with energy of about 2 MeV from electrostatic accelerator is focused into several μm probe, which scans over the sample surface. Such probe penetrates few tens of μm into the sample without its spreading and sample destruction.

* Corresponding author.
E-mail address: yaroslav.znamenshchykov@gmail.com (Y.V. Znamenshchykov).

http://dx.doi.org/10.1016/j.mssp.2017.02.004
Received 3 August 2016; Received in revised form 30 January 2017; Accepted 3 February 2017

Table 1
Studying of chemical composition of CZT films by EDS, XRD and PIXE methods.

Sample	EDS				XRD				PIXE			
	Concentration (at%)			x	Concentration (at%)			x	Concentration (at%)			x
	Cd	Zn	Te		Cd	Zn	Te		Cd	Zn	Te	
CZT1	33.8	21.3	44.9	0.39	34.5	15.5	50	0.31	31.3	18	50.7	0.37
CZT2	28.3	26.2	45.5	0.48	27	23	50	0.46	26.9	22.7	50.4	0.46
CZT3	19.3	34.4	46.3	0.64	17.5	32.5	50	0.65	15.9	33.8	50.3	0.68
CZT4	12.0	42.7	45.3	0.78	11.5	38.5	50	0.77	9.9	39.8	50.3	0.80

Therefore, μ-PIXE provides high-resolution elemental mapping of near-surface region with the detection limits of about 1–20 ppm.

The PIXE method was used for analysis of chemical composition and distribution of elements in compound and multicompound thin films [20–23]. But this method has not been used for analysis of CZT films.

The goal of this work is to study the effect of zinc concentration on structural properties of thick CZT films, obtained by close spaced vacuum sublimation (CSVS) method. Also, in order to determine the presence of secondary phases in thick CZT films with different Zn concentration the surface distribution of the chemical elements is established.

2. Experimental details

The CZT films were deposited on ITO-coated glass substrates by close-spaced vacuum sublimation method, which was described in our previous works [24–26]. The mixture of CdTe and ZnTe powders was used for evaporation; the total mass of evaporated powder was 100 mg. In order to obtain CZT films with different Zn concentration, the mass ratio (M_R) between cadmium telluride and zinc telluride powder has been varied as follows: 9, 2.3, 1 and 0.4 for CZT1, CZT2, CZT3 and CZT4 samples, respectively. The growth conditions for films were the same, namely, the substrate temperature was 400 °C and the evaporator temperature was 700 °C.

The surface morphology of the films has been investigated by REM-100 scanning electron microscope (SEM). The average grain size (D) of the layers was estimated by Jeffries method [27].

The chemical composition of the films was studied by energy dispersive spectroscopy (EDS) on the surface area of 200×200 μm. The measurement parameters were as follows: beam exposure of 100 s, beam energy of 20 keV. In order to achieve the highest signal-to-noise ratio, the average value of output signal intensity was adjusted to be of about 1000 counts/sec. It should be noted that surface of the samples was not etched or polished for more precise EDS measurements, and the surface of the film was assumed to be flat. However, the roughness of the film could lead to increasing in error of quantitative EDS analysis up to 5% [28].

The chemical composition of the samples was also studied by particle-induced X-ray emission μ-PIXE technique using the scanning nuclear microprobe. After collimation the proton beam of energy of 1 MeV was focused on 5×5 μm area of the sample. The beam was scanned across the geometrical raster of 250 μm×250 μm. The X-ray emission signal generated from each pixel was collected by Amptek XR-100CR Si (Li) X-ray detector with Be window of 25.4 μm thickness positioned at 135° to the incident beam direction. That allows to obtain two-dimensional maps of spatial distribution of concentration of compound elements. General PIXE spectra from each scanned area were processed by using the GUPIX software [29] to quantify the elemental composition of the samples.

The X-ray diffraction (XRD) analysis was used to study the structural properties of the layers. The measurements of XRD spectra were carried out by DRON 4–07 diffractometer in a conventional Bragg-Brentano θ–2θ geometry (2θ is the Bragg's angle) using Ni-filtered CuK_α radiation (λ=0.15406 nm). The samples were measured in the 2θ angle range from 20° to 80°. The peak intensities were normalized to the intensity of (111) peak of the cubic phase. Phase analysis was performed by comparison of the inter-planar distances as well as relative intensities measured from the samples with reference Joint Committee on Powder Diffraction Standards (JCPDS card No. 15–0770) data [30]. Precise values of the lattice parameter were determined by the extrapolated Nelson–Riley method [31].

Room temperature Raman spectra were studied using semiconductor IR (λ=785 nm) and an Ar (λ=514 nm) lasers as an excitation source. Measurement parameters were the same as in previous work [32].

3. Results and discussion

The study of chemical composition by EDS method shows that CZT films have following Zn concentrations: 21.3 at%, 26.2 at%, 34.4 at% and 42.7 at% for the CZT1, CZT2, CZT3 and CZT4 samples, respectively. Thus, Zn concentration is expectedly increasing with decreasing of M_R. The results of the films chemical composition study are presented in Table 1.

The SEM images of the surface of CZT films are shown in Fig. 1. The CZT1 sample consists of well-faceted grains with smooth flat surfaces (Fig. 1(a)) and the size of grains (D) is ranged from 10 to 22 μm (Fig. 1(a)). The investigation the surface of CZT2 sample shows irregular grains with D of about 8 μm (Fig. 1(b)). The surface of CZT3 sample includes non-uniform grains with D of 3 μm, most grains contain sub-grains with the size of about 1 μm (Fig. 1(c)). The shape of grains of CZT4 sample is very similar to those in CZT2 sample, whereas D value of 3.5 μm was almost twice smaller (Fig. 1(d)). Thus, the concentration dependence of surface quality in CZT films has a non-linear character. With increasing of x from 0.37 to 0.68 deterioration of surface was observed, with further increasing of x from 0.68 to 0.80 the surface morphology of the films shows improvement.

The changes of the film surface morphology could be caused by two factors:

1) Deformation of the crystal lattice due to increasing amount of Zn atoms similarly to CZT single crystals [33,34], where relationship of crystalline quality of CZT from x was described by parabola with the minimum at x=0.5.
2) The effect of the growth conditions on properties of CZT films. In particular, chosen growth conditions (T_s=400 °C, T_e=700 °C) are more equilibrium for deposition of Zn-poor films (CZT1 and CZT2) than for Zn-rich films (CZT3 and CZT4). This could be explained by the fact that sublimation temperature of ZnTe is higher than of CdTe. It leads to the decreasing of vapour pressure above the evaporator and substrate (the vapour above the substrate consists of gas flux from the evaporator and re-evaporated gas from the substrate [35]). Thus the level of saturation of vapour in a close-spaced sublimation chamber is decreased with the amount of Zn in initial powder.

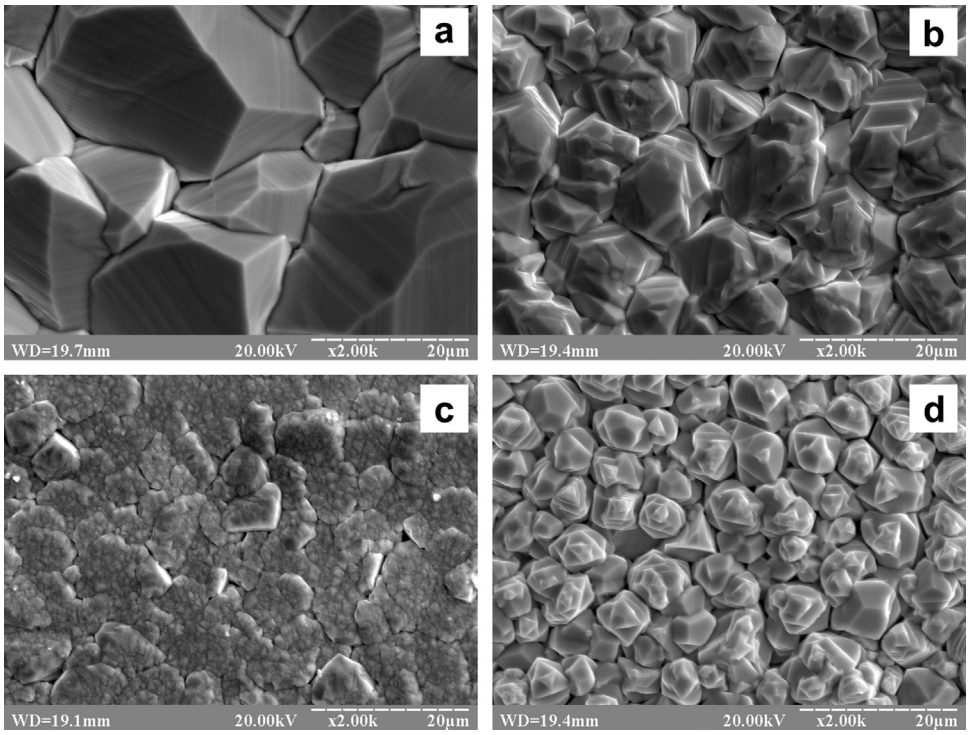

Fig. 1. SEM images of CZT samples surface: (a) CZT1 (x=0.37), (b) CZT2 (x=0.46), (c) CZT3 (x=0.68), (d) CZT4 (x=0.80).

As it was determined from the cross-section of the sample, the thicknesses of the samples were about 60 μm.

The XRD patterns of the CZT1-CZT4 films are presented in Fig. 2.

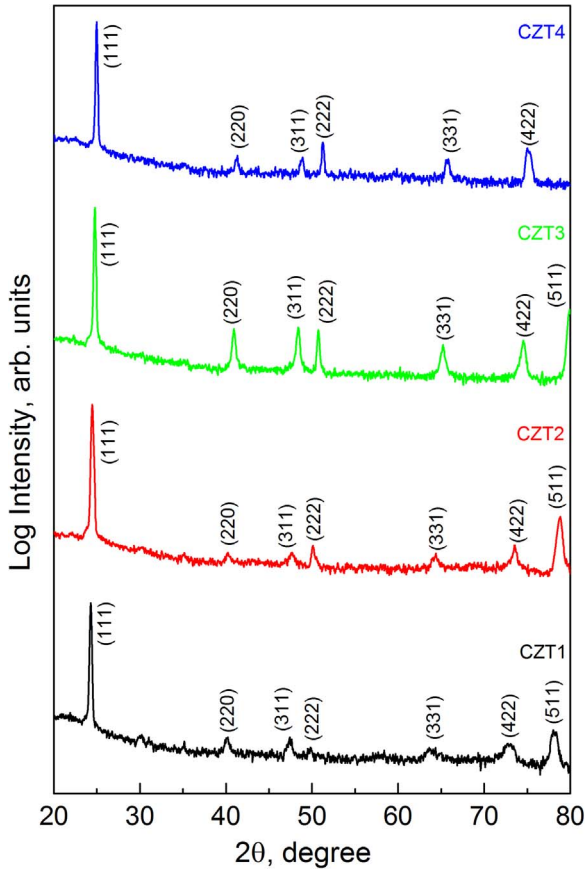

Fig. 2. XRD patterns of CZT1 (x=0.37), CZT2 (x=0.46), CZT3 (x=0.68) and CZT4 (x=0.80) samples.

The reflections from (111), (220), (311), (222), (422), (331) and (511) planes of the cubic (zinc-blende) phase of CZT are observed on the patterns [30]. The dominant (111) peak correspond to preferential growth orientation along [111] direction. The peaks of other crystal phases such as hexagonal phase of CZT were not observed. This indicates single-phase cubic structure of the samples. Analogously to our previous works [32,36], with increasing of Zn concentration the diffraction peaks are shifting towards higher values of diffraction angles due to decreasing lattice parameter.

As it is seen from Fig. 2, the XRD peaks are sharp and symmetrical, which could be considered as an evidence of high homogeneity and crystal quality of the samples. In contrast to our work [32], where splitting of diffraction peaks was observed in Zn-rich CZT films, the diffraction peaks in Fig. 2 are not splitted, which indicates homogenous bulk distribution of Zn atoms in the sample. These results allow us to conclude that evaporation of mixture of CdTe and ZnTe powders, is more preferable for deposition of homogeneous CZT films, than co-evaporation of CdTe and ZnTe powders from two different sources performed in our previous work [32].

The values of the lattice parameter of CZT films were found to be 0.63623, 0.63048, 0.62323 and 0.61845 nm for the CZT1, CZT2, CZT3 and CZT4 samples, respectively. These values were used for calculation of x in $Cd_{1-x}Zn_xTe$ samples by the Vegard's law [33]. The results of the calculations are listed in Table 1.

Typical summary PIXE spectra, obtained after irradiation of random regions of the surface of CZT samples with a proton beam are presented in the Fig. 3. According to SRIM (Stopping and Range of Ions in Matter) simulation [37], the penetration depth of protons is about 11–12 μm. As it is seen from Fig. 3, only lines from the components of solid solution (Cd, Zn, Te) were observed on spectra, which is the evidence of high chemical purity of the films (resolution of the method is 3×10^{-4}). Analysis of characteristic spectra (PIXE) allowed us to determine chemical composition of layers (Table 1). As it is seen from Table 1, values of atomic concentration of Zn, obtained by PIXE, are slightly lower than values, obtained by EDS and XRD. But at the same time values of atomic concentrations of components, obtained by PIXE, EDS and XRD, are well-correlated. Since PIXE

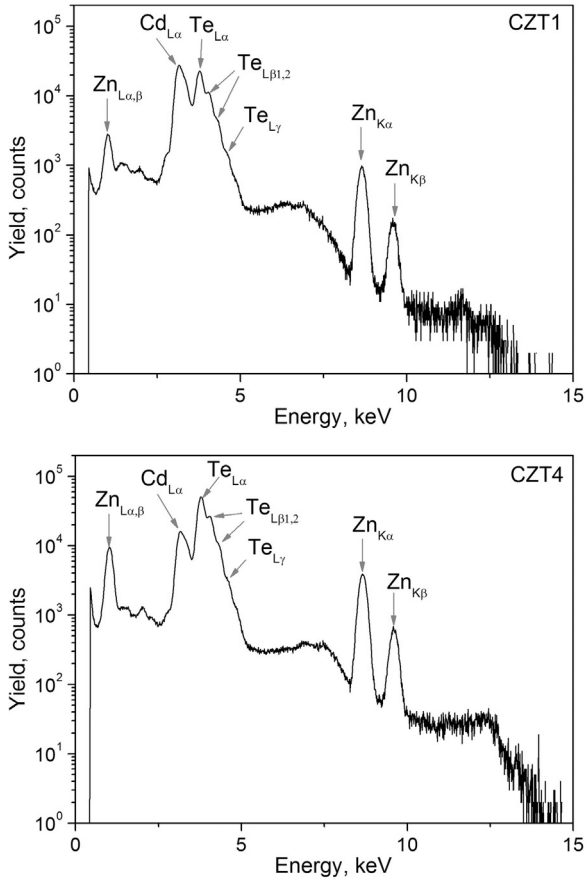

Fig. 3. Summed PIXE spectra from the CZT1 (x=0.37) and CZT4 (x=0.80) samples.

method is the most accurate (the error in determining of concentrations does not exceed 0.67%), values of concentrations of components, obtained by this method, are the most precise.

In order to evaluate distribution of elements in the film, scanning of samples surface by proton beam (μ-PIXE) was carried out. Maps of Zn distribution (Fig. 4) were obtained after spectra treatment using Zn K-α line with the energy of 8.64 keV, which is sufficiently resolved with no interferences. Processing of Cd L-α line with the energy of 3.13 keV and Te L-α line with 3.77 keV allowed to determine distribution of Cd and Te atoms, corresponding maps for CZT2 and CZT4 samples are presented in Fig. 4. The scale bars show quantity of output quanta of characteristic X-rays, induced by focused proton beam, in the range of energy which corresponds to K-line (Zn) and L-line (Cd and Te) in the PIXE spectrum (Fig. 3). The scale bars show normalized values of signal output using conditional colors, therefore numerical values are not presented. It was established that difference in quantity of output quanta of characteristic X-rays in each pixel of maps is in the range of statistical straggling, therefore it can be stated that components of solid solution are quite uniformly distributed on the surface of films.

Thereby, μ-PIXE analysis has established that chemical composition of CZT solid solution is uniform in the surface of samples, the obtained films don't contain Te, Cd and Zn precipitates.

The values of x for EDS and PIXE measurements (Table 1) were calculated as a ratio of Zn concentration to sum of Zn and Cd concentrations. As it is seen from the Table 1, some disagreement between values of Zn concentration obtained from EDS, XRD and PIXE study is observed. This could be caused by through-thickness inhomogeneity of Zn concentration in the CZT films. In turn, since the penetration depth of X-ray probe of EDS, X-rays of XRD and protons beam of PIXE method is different the values of Zn concentration obtained by these methods could be also different. Another reason for such disagreement is that accuracy of EDS measurements of non-polished samples with a high surface roughness could reach 5% [28].

Room-temperature Raman spectra of CZT films with different Zn concentration are presented on Fig. 5. The spectra were measured using 785 and 514 nm laser excitation wavelengths. It should be noted that we were not able to obtain Raman spectra of CZT3 and CZT4 samples using laser excitation of 514 nm, because of high background luminescence also similar to works [16,38] on the Raman spectra measured with laser excitation of 514 nm the Te-related peaks were observed. This is due to local overheating and evaporation of Cd atoms and hence Te-enrichment of the surface. Therefore for the further analysis the spectra measured with laser excitation of 785 nm were used. The power laser excitation radiation and exposure time were chosen so as to obtain high signal-to-noise ratio while avoiding damage to the surface and high background luminescence. Thus, application of laser excitation with power density of 6 W/cm^2 and exposure time of 20 s allows good quality spectra for all samples except CZT2. In the case of CZT2 sample, application of laser excitation with power density of 6 W/cm^2 caused high background luminescence. The decreasing of the power density to 0.06 W/cm^2 allows to avoid background luminescence but the quality of the spectrum was low. The improvement of quality of the spectrum was possible only with the substantial increasing of the exposure time from 20 to 3600 s.

According to works [18,39–41], the modes of CdTe and ZnTe in CZT Raman spectra are shifted from those position in pure compounds depending on Zn concentration. In particular, with increasing of Zn concentration the frequency of LO_1(CdTe) mode is decreasing [39,40], while frequencies of TO_1(CdTe), LO_2(ZnTe), TO_2(ZnTe) modes are increasing. At the same time, the Raman shift of LO and TO modes are highly and weakly dependent on x, respectively. In works [39–41], the compositional dependencies of frequencies of CdTe and ZnTe-like modes are presented. These dependencies are plotted on Fig. 6 and were used for the identification of the Raman modes in the present study. It should be noted that the analysis of influence of chemical composition on frequencies of Raman modes was performed according to x values obtained by PIXE method, since this method provides the most accurate values of x.

The strongest mode at 177 cm^{-1} on the Raman spectrum of CZT1 measured with a 785 nm excitation could be assigned with TO_2(ZnTe), as the frequency of this mode is in a good correlation with the value which could be obtained from reference curve for the x=0.37 (Fig. 6). The TO_2(ZnTe) mode is also observed in the Raman spectra of the CZT2, CZT3 and CZT4 samples at 179, 180 and 181 cm^{-1} (Fig. 5). It should be noted that these values are well correlated with the frequency vs. x reference data (Fig. 6). Thus, analogously to works [39,40], the frequency of TO_2(ZnTe) mode is weakly dependent on x (Fig. 6). According to reference data, the frequency of LO_2(ZnTe) mode for the x=0.37 (CZT1 sample) is about 191 cm^{-1} (Fig. 6). In a case of CZT1 sample this mode is not clearly distinguishable. However, asymmetrical shape of the TO_2(ZnTe) peak implies the presence of LO_2(ZnTe) mode on its shoulder at about 189 cm^{-1} (Fig. 5). This assumption is supported by the observed exponential increasing of the frequency and relative intensity of this mode with x for the CZT2, CZT3 and CZT4 samples (Figs. 5 and 6). The frequency of LO_2(ZnTe) mode of CZT1, CZT2, CZT3 and CZT4 samples is less than reference values, which could be explained by the presence of extended effects in polycrystalline films. According the reference data presented on Fig. 6, the peak at 155 cm^{-1} on Raman spectrum of the CZT1 sample can be assigned with both TO_1(CdTe) and LO_1(CdTe) modes. However, in work [42], oscillation mode at 153 cm^{-1} in Raman spectra of $Cd_{1-x}Zn_xTe$ crystal with x=0.10 was identified as TO_1(CdTe) mode, so taking into account increasing of frequency of TO_1(CdTe) mode with x we assign the peak at 155 cm^{-1} on Raman spectrum of the CZT1 with TO_1(CdTe) mode. Peak at about 160 cm^{-1} on the Raman spectra of the CZT2, CZT3 and CZT4 samples can be clearly identified as LO_1(CdTe) mode, since the frequencies of this mode measured for the above mentioned samples are in a good correlation with the reference data (Fig. 6). Similar to

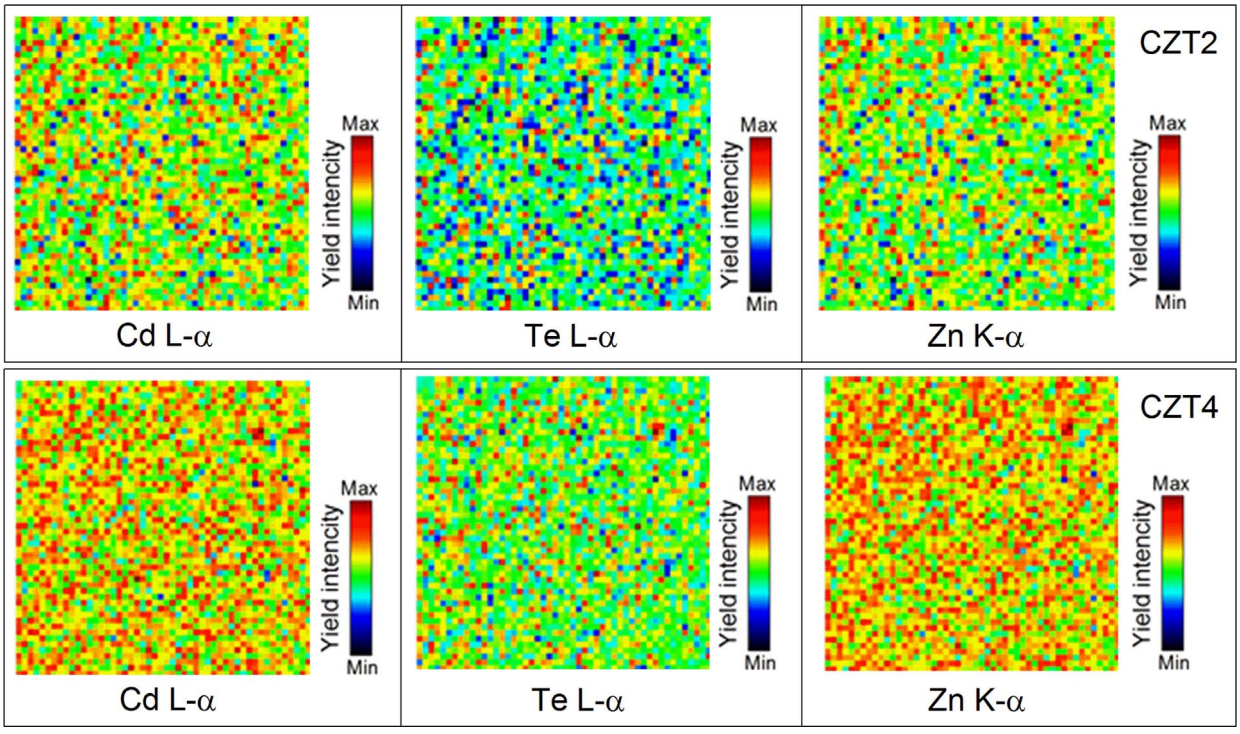

Fig. 4. The μ-PIXE maps of elemental distributions in CZT2 (x=0.46) and CZT4 (x=0.80) samples from the scanned area 250×250 μm^2 and surface layer thickness about 11 μm.

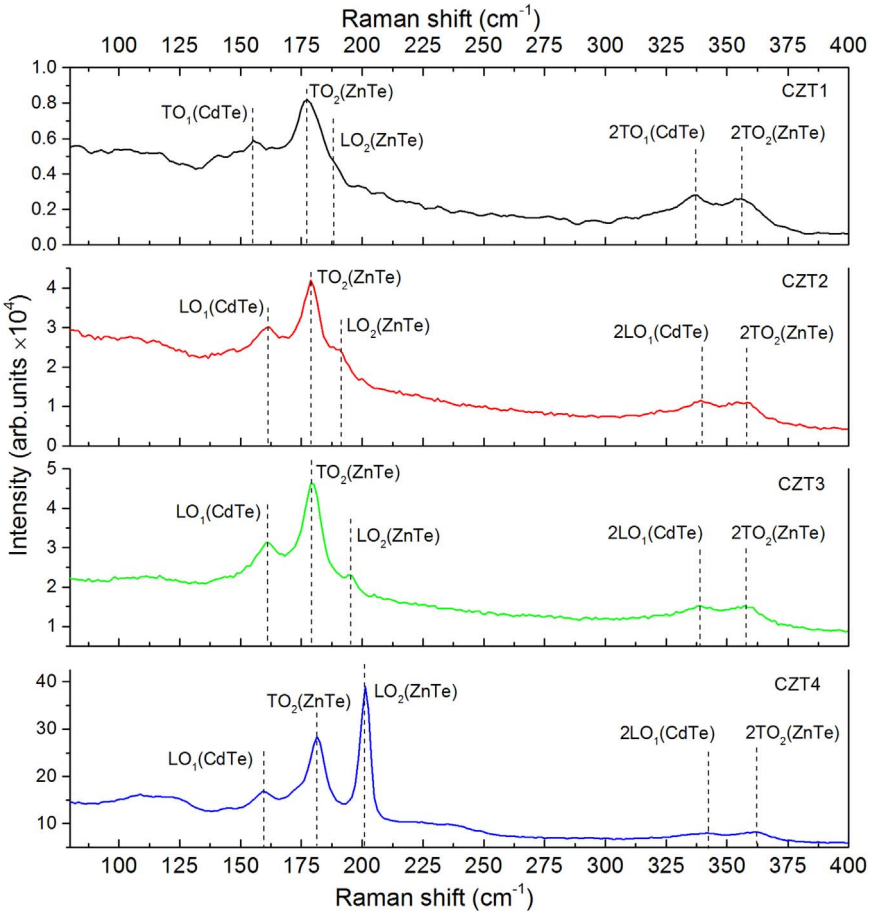

Fig. 5. Room temperature Raman spectra of the CZT1 (x=0.37), CZT2 (x=0.46), CZT3 (x=0.68), CZT4 (x=0.80) samples, measured with 785 nm excitation.

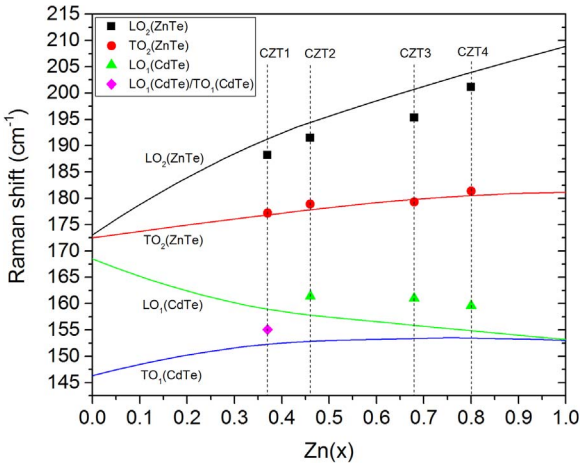

Fig. 6. The compositional dependencies of frequencies of CdTe and ZnTe-like modes. Solid lines-reference data [40], dots – experimental results.

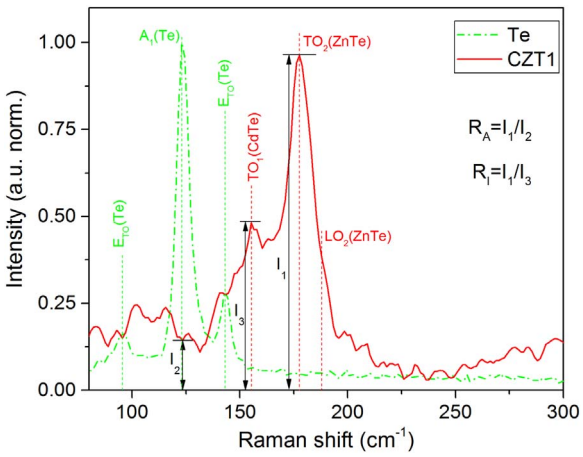

Fig. 7. Raman spectra of the Te crystal (dash-dot line) and CZT1 (x=0.37) sample (solid line).

works [39–41], the frequency of this mode is slightly decreased with x (Figs. 5 and 6).

Also, Raman spectra of CZT films show second-order phonons, namely, on the spectrum of CZT1 sample $2TO_1$(CdTe) and $2TO_2$(ZnTe) modes were observed, spectra of CZT2-CZT4 samples include $2LO_1$(CdTe) and $2TO_2$(ZnTe) resonant overtones. It is due resonant enhancement of the RS signal, since value of incoming excitation energy E_{in} of IR laser (E=1.579 eV) is close to fundamental bandgap of the material [39,43]. As it is seen from Fig. 5, the $2TO_1$(CdTe) and $2TO_2$(ZnTe) modes on the spectrum of CZT1 sample have relatively high intensity, while on the spectrum of CZT4 sample shallow peaks at 342 and 361 cm^{-1} were assigned to $2LO_1$(CdTe) and $2TO_2$(ZnTe) modes, respectively. Decreasing of resonant overtones intensity is explained by increasing of bandgap of CZT with Zn concentration, hence resonance conditions are not fully satisfied in Zn-rich films at 785 nm excitation.

The clear observation of CdTe and ZnTe-related modes on Raman spectra makes it possible to carry out the detailed phase analysis and to study spatial phase distribution in samples. With this purpose, we performed micro-Raman mapping of the samples surface. As was mentioned above in a case of CZT2 sample the exposure time for the obtaining of Raman spectrum was rather long, namely 3600 s. Thus we were not able to carry out micro-Raman mapping for the CZT2 sample.

In order to establish position of the Te-related modes the Te crystal was measured under the same conditions as CZT samples, namely wavelength of laser radiation of 785 nm, power density of 6 W/cm^2 and exposure time of 20 s. As could be seen in Fig. 7, the Raman spectrum of Te crystal shows typical intensive peak due to A_1 symmetry phonon at 122 cm^{-1} and two E_{TO} modes at 95 and 143 cm^{-1} [44,45]. Thus, as a parameter indicating presence of Te secondary phase the ratio (R_A) of the intensity (I_1) of dominant peak related to TO_2(ZnTe) mode to the intensity (I_2) of Raman signal at around 122 cm^{-1} (reference frequency of A_1(Te) mode) was considered (Fig. 7).

The possible formation of the inclusions of pure ZnTe and CdTe was studied using the micro-Raman mapping of R_I parameter, which is the ratio (R_I=I_1/I_3) of TO_2(ZnTe) mode and the strongest CdTe- related mode (TO_1(CdTe) for CZT1 sample, and LO_1(CdTe) for CZT3, CZT4 samples) intensities as it shown in Fig. 7. Thus, we choose the most intensive and clearly distinguishable modes for the analysis.

It should be noted that the background luminescence, Rayleigh and surface scattering could lead to raised level of the baseline of the Raman spectra, and hence misinterpretation of results related to intensities of peaks. Therefore we performed baseline correction for all Raman spectra.

The surface distribution of R_A parameter for the CZT1 sample is presented on Fig. 8(a). As could be seen from Fig. 8(a), the R_A parameter for CZT1 sample is changed from 3 to 25, and dispersion from the mean of R_A is 11. We assumed that for the points with $R_A > 7$ the presence of Te inclusions is improbable since the I_1 intensity is significantly higher than I_2. For example, as could be seen from Fig. 8(a), the I_2 intensity on the Raman spectrum of the point with R_A=24.5 does not exceed the background level. In terms of identification of Te inclusions, the points with the minimal R_A should be considered. However, the analysis of the Raman spectrum of the point with R_A=2 shows that the increasing of I_2 intensity is due to raised level of background.

A similar result was obtained for the CZT3 sample for which the dispersion from the mean of R_A is about 2, namely, the Raman spectra of points with maximal and minimal R_A value of 7.8 and 3.8, respectively, show that R_A is decreasing with increasing level of background. And the Te-related modes are not clearly visible on spectrum of point with R_A=3.7.

The mapping of CZT4 sample show dispersion from the mean of R_A parameter of only 1.8. Thus the relative intensities I_1 and I_2 for the points with maximal and minimal R_A of 6.5 and 2.9, respectively, are similar. The R_A is varied with intensity of broad peak centered at 118 cm^{-1}. Despite the fact the frequency of this broad peak is close to reference frequency of Te- related modes, it is difficult to associate it with Te inclusions, since the Te- related modes are not clearly distinguishable on spectra.

The mapping of R_I parameter for the CZT1 sample is presented in Fig. 8(b). As could be seen from Fig. 8(b), the dispersion from the mean of R_I parameter for CZT1 sample is 0.6. Values of the dispersion from the mean of R_I parameter for CZT3 and CZT4 were 0.25 and 0.5, respectively. In a case of CZT4 sample, the distribution of R_I was rather uniform and agglomerations of points with similar R_I were not observed, while on the mapping of CZT1 sample the agglomerations of points with R_I of about 1.4 and 2.5 were visible. Also, the agglomerations of points with R_I of about 1.7 and 2.2 were observed on mapping of CZT3 sample. The analysis of spectra measured for points from these agglomerations does not show presence of pure secondary phases of CdTe or ZnTe. We speculate that such agglomerations could take place, because of some local deviation of metal concentration from the mean value. But also it could be due to variation of background level caused by the effect of the surface roughness on the scattering of laser radiation.

Taking into account that the highest value of dispersion from the mean of R_A and R_I corresponds to the CZT1 sample with biggest grains size, we assumed that R_A is varied because of effect of surface roughness on scattering of laser excitation radiation, rather than presence of secondary phases.

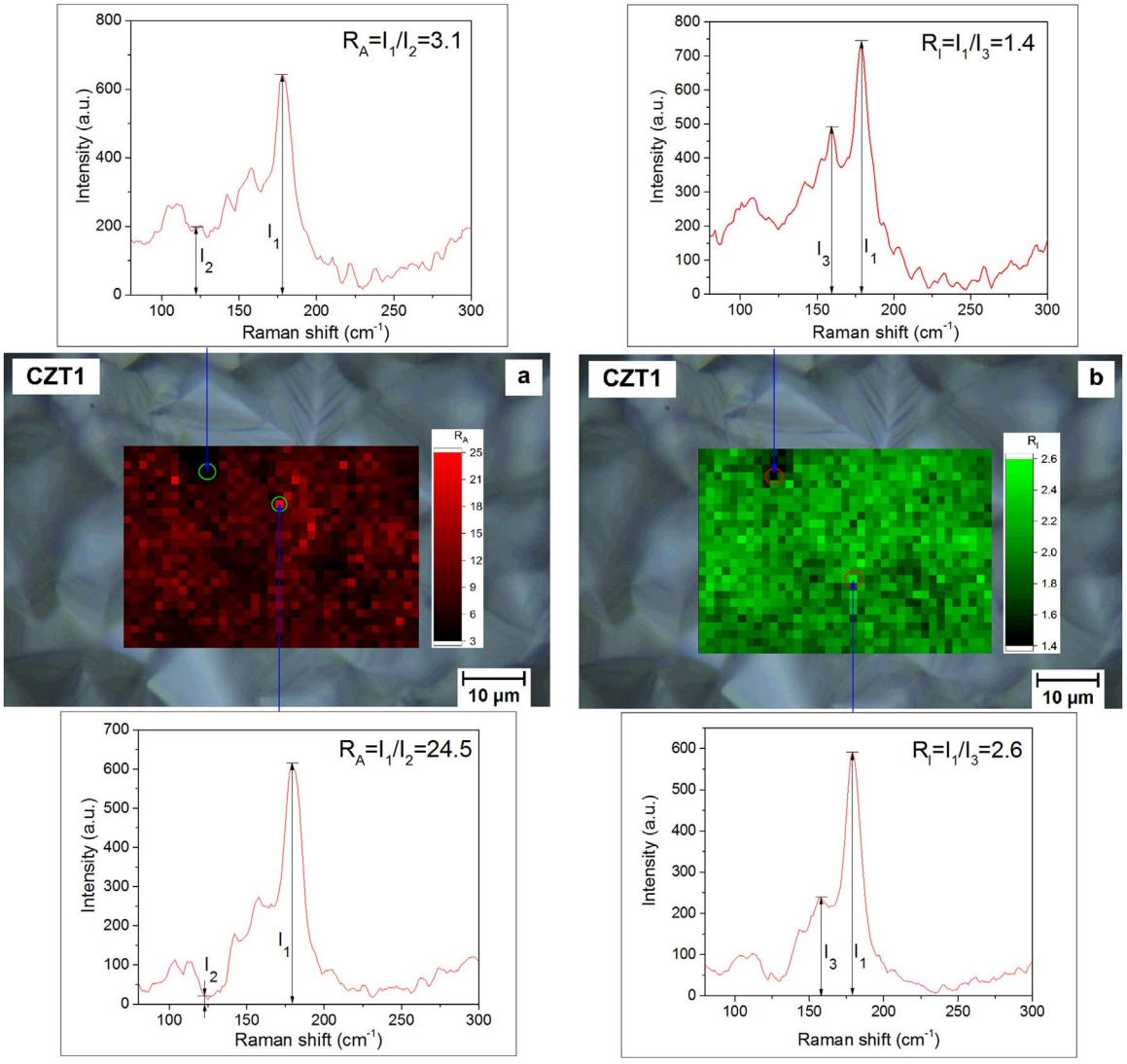

Fig. 8. Raman mapping of R_A (a) and R_I (b) parameters of CZT1 (x=0.37) sample.

4. Conclusion

In this work, thick polycrystalline $Cd_{1-x}Zn_xTe$ films with $x > 0.30$, obtained by CSVS method, were investigated. Structural analysis showed that samples consist of only cubic zinc blende phase. The diffraction peaks are sharp and symmetrical, which indicates high homogeneity and crystal quality of the films. The concentration dependence of surface quality in CZT films has a non-linear character, which could be caused by deformation of crystal lattice with introduction of Zn atoms, as well as non-optimal growth conditions for Zn-rich films. Zn concentration in CZT films was determined by EDS, PIXE, and was calculated by the Vegard's law from the lattice parameter. Study of phase composition by Raman spectroscopy showed that Raman spectra of CZT samples include only CdTe- and ZnTe-like LO and TO modes, which indicates the absence of secondary phases on the films surface.

We show that micro-Raman and PIXE mappings are suitable for analysis of the surface distribution of chemical components. As follows from PIXE and micro-Raman joint study, the components of CZT solid solution are uniformly distributed on the film surface. Secondary phases, such as CdTe, ZnTe, Cd, Zn, and Te inclusions, were not found.

Thus, it was determined, that CSVS method allows to obtain high-quality thick polycrystalline CZT films with $x > 0.30$ and uniform bulk distribution of components of the film for application in hard radiation detectors.

Acknowledgments

This work was supported by Erasmus Ianus Programme (Grant Agreement Number 2013 – 2524/ 001 – 001 – EMA2), Latvian National Research Programme in Materials Science (IMIS2) (2014-2017) and by the Ministry of Education and Science of Ukraine (Grant No. 0115U000665c, No. 0116U002619).

References

[1] S. del Sordo, L. Abbene, E. Caroli, A.M. Mancini, A. Zappettini, P. Ubertini, Progress in the development of CdTe and CdZnTe semiconductor radiation detectors for astrophysical and medical applications, Sensors 9 (2009) 3491–3526. http://dx.doi.org/10.3390/s90503491.

[2] A. Owens, Compound Semiconductor Radiation Detectors, CRC Press, Boca Raton, 2012.

[3] M. Fiederle, T. Feltgen, J. Meinhardt, M. Rogalla, K.W. Benz, State of the art of (Cd,Zn)Te as gamma detector, J. Cryst. Growth 197 (1999) 635–640. http://dx.doi.org/10.1016/S0022-0248(98)00761-1.

[4] C. Szeles, M.C. Driver, Growth and properties of semi-insulating CdZnTe for radiation detector applications, Proc. SPIE - Int. Soc. Opt. Eng. 3446 (1998) 2–9. http://dx.doi.org/10.1117/12.312878.

[5] G. Li, W. Jie, Z. Gu, H. Hua, Growth of $Cd_{1-x}Zn_xTe$ crystals with different x values and their qualities comparison, J. Cryst. Growth 263 (2004) 332–337. http://dx.doi.org/10.1016/j.jcrysgro.2003.11.069.

[6] P.J. Sellin, Thick film compound semiconductors for X-ray imaging applications,

Nucl. Instrum. Methods Phys. Res. Sect. A: Accel. Spectrom., Detect. Assoc. Equip. 563 (2006) 1–8. http://dx.doi.org/10.1016/j.nima.2006.01.110.
[7] J. Takahashi, K. Mochizuki, K. Hitomi, T. Shoji, Growth of $Cd_{1-x}Zn_xTe$(x~0.04) films by hot-wall method and its evaluation, J. Cryst. Growth 269 (2004) 419–424. http://dx.doi.org/10.1016/j.jcrysgro.2004.05.054.
[8] S. Tokuda, H. Kishihara, S. Adachi, T. Sato, Preparation and characterization of polycrystalline CdZnTe films for large-area, high-sensitivity X-ray detectors, J. Mater. Sci. Mater. Electron. 15 (2004) 1–8. http://dx.doi.org/10.1023/A:1026297416093.
[9] J. Tao, H. Xu, Y. Zhang, H. Ji, R. Xu, J. Huang, J. Zhang, Xi Liang, K. Tang, L. Wang, Interface chemistry of CdZnTe films studied by a peel-off approach, Appl. Surf. Sci. (2016) 1–5. http://dx.doi.org/10.1016/j.apsusc.2016.01.245.
[10] Yuk, S., Park, S.W., Yi, Y., 2006. Polycrystalline CdZnTe thick films for low energy X-ray: System evaluation. Proceedings of the IEEE Annual International Confrence Engineering in Medicine and Biology 1990–1993. doi:10.1109/IEMBS.2006.260666
[11] S. Kang, B. Jung, S. Noh, C. Cho, I. Yoon, J. Park, Feasibility study of direct-conversion x-ray detection using cadmium zinc telluride films, J. Instrum. 7 (2012) C01010. http://dx.doi.org/10.1088/1748-0221/7/01/C01010.
[12] J. Min, X. Liang, J. Chen, D. Wang, H. Li, J. Zhang, Investigation of Te inclusions in CdZnTe crystalline material using Raman spectroscopy and IR techniques, Vacuum 86 (2012) 1003–1006. http://dx.doi.org/10.1016/j.vacuum.2011.11.009.
[13] P. Fochuk, R. Grill, O. Kopach, A.E. Bolotnikov, E. Belas, M. Bugar, G. Camarda, W. Chan, Y. Cui, A. Hossain, K.H. Kim, I. Nakonechnyi, O. Panchuk, G. Yang, R.B. James, Elimination of Te inclusions in $Cd_{1-x}Zn_xTe$ crystals by short-term thermal annealing, IEEE Trans. Nucl. Sci. 59 (2012) 256–263. http://dx.doi.org/10.1109/TNS.2012.2187069.
[14] G. Yang, A.E. Bolotnikov, Y. Cui, G.S. Camarda, A. Hossain, K.H. Kim, R. Gul, R.B. James, Low-temperature spatially resolved micro-photoluminescence mapping in CdZnTe single crystals, Appl. Phys. Lett. 98 (2011) 25–28. http://dx.doi.org/10.1063/1.3603930.
[15] G.A. Kulkarni, V.G. Sathe, K.S.R.K. Rao, D.V.S. Muthu, R.K. Sharma, Micro-Raman imaging of Te precipitates in CdZnTe (Zn~4%) crystals, J. Appl. Phys. 105 (2009). http://dx.doi.org/10.1063/1.3086274.
[16] S.A. Hawkins, E. Villa-Aleman, M.C. Duff, D.B. Hunter, A. Burger, M. Groza, V. Buliga, D.R. Black, Light-induced tellurium enrichment on CdZnTe crystal surfaces detected by Raman spectroscopy, J. Electron. Mater. 37 (2008) 1438–1443. http://dx.doi.org/10.1007/s11664-008-0448-x.
[17] E. Bilgilisoy, S. Özden, E. Bakali, M. Karakaya, Y. Selamet, Characterization of CdTe Growth on GaAs Using Different Etching Techniques, J. Electron. Mater. 44 (2015) 3124–3133. http://dx.doi.org/10.1007/s11664-015-3830-5.
[18] A. Aydinli, A. Compaan, G. Contreras-Puente, Polycrystalline $Cd_{1-x}Zn_xTe$ thin films on glass by pulsed laser deposition, Solid State Commun. 80 (1991) 5–8.
[19] D.V. Magilin, A.G. Ponomarev, V.A. Rebrov, N.A. Sayko, K.I. Melnik, V.I. Miroshnichenko, V.Y. Storizhko, Performance of the Sumy nuclear microprobe with the integrated probe-forming system, Nucl. Instrum. Methods Phys. Res. Sect. B: Beam Interact. Mater. Atoms 267 (2009) 2046–2049. http://dx.doi.org/10.1016/j.nimb.2009.03.015.
[20] J.P. Nair, R. Jayakrishnan, N.B. Chaure, A. Lobo, S. Kulkarni, R. Pandey, B. Kanngießer, B. Beckhoff, M. Jaksic, N.P. Barradas, Investigation of Sb-doped CdTe films using XPS, PIXE and XRD, Thin Solid Films. 347 (1999) 39–45. http://dx.doi.org/10.1016/S0040-6090(98)01408-4.
[21] A. Karydas, I. Bogdanovic Radovic, C. Streeck, C. Kaufmann, R. Caballero, T. Rissom, B. Kanngießer, B. Beckhoff, M. Jaksic, N.P. Barradas, In-depth elemental characterization of Cu(In,Ga)Se2 thin film solar cells by means of RBS and PIXE techniques, Nucl. Instrum. Methods Phys. Res. Sect. B: Beam Interact. Mater. Atoms 331 (2014) 93–95. http://dx.doi.org/10.1016/j.nimb.2014.01.025.
[22] A.G. Karydas, C. Streeck, I. Bogdanovic Radovic, C. Kaufmann, T. Rissom, B. Beckhoff, M. Jaksic, N.P. Barradas, Ion beam analysis of $Cu(In,Ga)Se_2$ thin film solar cells, Appl. Surf. Sci. 356 (2015) 631–638. http://dx.doi.org/10.1016/j.apsusc.2015.08.133.
[23] D. Nam, A.S. Opanasyuk, P.V. Koval, A.G. Ponomarev, A.R. Jeong, G.Y. Kim, W. Jo, H. Cheong, Composition variations in $Cu_2ZnSnSe_4$ thin films analyzed by X-ray diffraction, energy dispersive X-ray spectroscopy, particle induced X-ray emission, photoluminescence, and Raman spectroscopy, Thin Solid Films. 562 (2014) 109–113. http://dx.doi.org/10.1016/j.tsf.2014.03.079.
[24] Y.P. Gnatenko, P.M. Bukivskij, I.O. Faryna, A.S. Opanasyuk, M.M. Ivashchenko, Photoluminescence of high optical quality CdSe thin films deposited by close-spaced vacuum sublimation, J. Lumin. 146 (2014) 174–177. http://dx.doi.org/10.1016/j.jlumin.2013.09.070.
[25] A.S. Opanasyuk, D.I. Kurbatov, V.V. Kosyak, S.I. Kshniakina, S.N. Danilchenko, Characteristics of structure formation in zinc and cadmium chalcogenide films deposited on nonorienting substrates, Crystallogr. Rep. 57 (2012) 927–933. http://dx.doi.org/10.1134/S1063774512070206.
[26] C.J. Panchal, A.S. Opanasyuk, V.V. Kosyak, M.S. Desai, I.Y. Protsenko, Structural and substructural properties of the zinc and cadmium chalcogenides thin films (A review), J. Nano- Electron. Phys. 3 (2011) 274–301.
[27] G.F. Vander Voort, Metallography: principles and practice, ASM International, New York, 1999.
[28] J. Goldstein, D.E. Newbury, D.C. Joy, C.E. Lyman, P. Echlin, E. Lifshin, L. Sawyer, J.R. Michael, Scanning Electron Microscopy and X-ray Microanalysis, Third edition, Springer Science & Business Media, 2012.
[29] J.L. Campbell, N.I. Boyd, N. Grassi, P. Bonnick, J.A. Maxwell, The Guelph PIXE software package IV, Nucl. Instrum. Methods Phys. Res. Sect. B: Beam Interact. Mater. Atoms. 268 (2010) 3356–3363. http://dx.doi.org/10.1016/j.nimb.2010.07.012.
[30] JCPDS, International Centre for Diffraction Data, USA, Card Number 15-0770.
[31] B.E. Warren, X-ray Diffraction, Dover, Mineola, NY, 1990.
[32] V. Kosyak, Y. Znamenshchykov, A. Čerškus, Y.P. Gnatenko, L. Grase, J. Vecstaudza, A. Medvids, A. Opanasyuk, G. Mezinskis, Composition dependence of structural and optical properties of $Cd_{1-x}Zn_xTe$ thick films obtained by the close-spaced sublimation, J. Alloy. Compd. 682 (2016) 543–551. http://dx.doi.org/10.1016/j.jallcom.2016.05.065.
[33] S. Stolyarova, F. Edelman, A. Chack, A. Berner, P. Werner, N. Zakharov, M. Vytrykhivsky, R. Beserman, R. Weil, Y. Nemirovsky, Structure of CdZnTe films on glass, J. Phys. D. Appl. Phys. 41 (2008) 065402. http://dx.doi.org/10.1088/0022-3727/41/6/065402.
[34] J.L. Reno, E.D. Jones, Determination of the dependence of the band-gap energy on composition for $Cd_{1-x}Zn_xTe$, Phys. Rev. B. 45 (1992) 1440–1442. http://dx.doi.org/10.1103/PhysRevB.45.1440.
[35] A. Lopez-Otero, Hot wall epitaxy, Thin Solid Films. 49 (1978) 3–57. http://dx.doi.org/10.1016/0040-6090(78)90309-7.
[36] V. Kosyak, Y. Znamenshchykov, A. Čerškus, L. Grase, Y.P. Gnatenko, A. Medvids, A. Opanasyuk, G. Mezinskis, Photoluminescence of CdZnTe thick films obtained by close-spaced vacuum sublimation, J. Lumin. 171 (2016) 176–182. http://dx.doi.org/10.1016/j.jlumin.2015.11.027.
[37] J.F. Ziegler, M.D. Ziegler, J.P. Biersack, SRIM – The stopping and range of ions in matter, Nucl. Instr. Meth. Phys. Res. B 268 (2010) 1818–1823. http://dx.doi.org/10.1016/j.nimb.2010.02.091.
[38] Y.L. Wu, Y.-T. Chen, Z.C. Feng, J.-F. Lee, P. Becla, W. Lu, Synchrotron radiation x-ray absorption fine-structure and Raman studies on CdZnTe ternary alloys, Hard X-Ray, Gamma-Ray, Neutron Detect, Phys. Xi. 7449 (2009) 74490Q–11. http://dx.doi.org/10.1117/12.825823.
[39] D.J. Olego, P.M. Raccah, J.P. Faurie, Compositional dependence of the Raman frequencies and line shapes of $Cd_{1-x}Zn_xTe$ determined with films grown by molecular-beam epitaxy, Phys. Rev. 33 (1986) 8–11. http://dx.doi.org/10.1103/PhysRevB.33.3819.
[40] S. Perkowitz, L.S. Kim, Z.C. Feng, Optical phonons in $Cd_{1-x}Zn_xTe$, Phys. Rev. B 42 (1990) 20–22.
[41] D.N. Talwar, Z.C. Feng, P. Becla, Impurity-induced phonon disordering in $Cd_{1-x}Zn_xTe$ ternary alloys, Phys. Rev. B 48 (1993) 17064–17071.
[42] A. Medvid', N. Litovchenko, A. Mychko, Y. Naseka, Exciton quantum confinement in nanocones formed on a surface of CdZnTe solid solution by laser radiation, Nanoscale Res. Lett. 7 (2012) 514. http://dx.doi.org/10.1186/1556-276X-7-514.
[43] J.F. Scott, R.C.C. Leite, T.C. Damen, Resonant Raman effect in semiconductors, Phys. Rev. 188 (1969) 1285–1290. http://dx.doi.org/10.1103/PhysRev.188.1285.
[44] P.M. Amirtharaj, F.H. Pollak, Raman scattering study of the properties and removal of excess Te on CdTe surfaces, Appl. Phys. Lett. 45 (1984) 789. http://dx.doi.org/10.1063/1.95367.
[45] A.S. Pine, G. Dresselhaus, Raman spectra and lattice dynamics of tellurium, Phys. Rev. B 4 (1971) 356–371. http://dx.doi.org/10.1103/PhysRevB.4.356.